

High-Throughput Computational Screening of Two-Dimensional Semiconductors

V. Wang,^{1,*} Y. Y. Liang,² Y. Kawazoe,³ and W. T. Geng^{4,†}

¹*Department of Applied Physics, Xi'an University of Technology, Xi'an 710054, China*

²*Department of Physics, Shanghai Normal University, Shanghai 200234, China*

³*New Industry Creation Hatchery Center, Tohoku University, Sendai, Miyagi 980-8579, Japan*

⁴*School of Materials Science & Engineering, University of Science and Technology Beijing, Beijing 100083, China*

(Dated: May 8, 2022)

By performing high-throughput calculations using van-der-Waals density-functional theory, we screen 120 direct- and 358 indirect-gap 2D nonmagnetic semiconductors from near 1000 2D monolayers according to energetic-, thermodynamic-, and mechanical-stability criterions. We present the calculated results including lattice constants, formation energy, Young's modulus, Poisson's ratio, band gap, band structure, ionization energy and electron affinity for all the systems satisfying our criterion.

I. INTRODUCTION

Since the successful isolation of graphene,^{1,2} two dimensional (2D) materials have attracted tremendous attentions due to their novel electronic, optical, thermal, and mechanical properties for potential applications in various fields. Due to the quantum confinement effect, 2D materials often exhibit unique features, different from those of their bulk counterparts.³⁻¹³ For examples, an unusual half-integer quantum Hall effect was observed in graphene.⁵ The layer-thickness depending on electronic properties of transition-metal dichalcogenides (TMDCs) with MX_2 composition (where $M = Mo$ or W and $X = S$, Se or Te) can be metallic or semiconducting.^{4,6,13-15} The peculiar puckered honeycomb structure of few-layer black phosphorus (phosphorene) leads to significant anisotropic electronic and optical properties on zigzag and armchair directions.^{12,16,17} Remarkably, its band gap is also thickness-dependent, varying from 0.3 eV in the bulk limit to ~ 2.2 eV in a monolayer with a direct band gap character. Other 2D materials, such as hexagonal boron nitride (h-BN),¹⁸ silicene,¹⁹⁻²² germanene,^{23,24} stanene,²⁵ also exhibit many exotic characteristics that are absent in their bulk counterparts.

A common feature of 2D materials is that they are formed by stacking layers with strong in-plane bonds and weak van der Waals (vdW) like interlayer attraction, allowing exfoliation into individual, atomically thin layers. Inspired by this feature, Inoshita *et al.* screened the potential two-dimensional binary stoichiometric electrides from the layered crystal structures by performing first principles calculations based on the density functional theory (DFT) within the generalized gradient approximation (GGA).²⁶ Later, Ahston and co-workers used a topology-scaling algorithm combining high throughput calculations,²⁷ to uncover more than 800 monolayers based on the Materials Project crystal structure databases²⁸. In parallel, Choudhary *et al.* identified at least 1300 monolayers by comparing the experimental lattice constants with those predicted at GGA level.²⁹ Specifically, it is well known that the semi-local density functionals such as GGA approach significantly overesti-

mates the lattice constants of crystals having vdW bonds. A rough thumb rule is that if the relative error in lattice constant a or b or c (experimental versus PBE-calculated) of one bulk phase is larger than 5%, it might have 2D structure. Another important database for 2D materials was builded by Mounet *et al.*³⁰ They chose the binding energy obtained by DFT calculations together with vdW correction, as the screening criterion (\leq few tens of meV· \AA^{-1}) and identified more than 1800 structures.

There are several 2D crystals databases publicly available nowadays.^{27,29,30} However, one of the major limitations of these databases mainly focus on the stability analysis to identify new stable structures using different algorithms. Furthermore, they only provide the fundamental physical properties such as lattice constants, formation energy, exfoliation energy and band gap at the GGA-level. It is well known that GGA can provide sufficiently accurate results on forces (near equilibrium), structures, and band dispersion, but underestimates band gaps, averagely 50%. A promising alternative approach is the replacement of GGA functionals by hybrid functionals. By including part of the exchange energy in a nonlocal manner in self-consistent calculations, they remedy the band gaps close to the experimental values.³¹⁻³³

In this work, combined high-throughput first-principles calculations with the existing 2D crystal structures databases mentioned above, we chose the thermodynamic-, mechanical-stability and conductivity type as criterions and screen around 478 2D semiconductors from near 1000 2D structures. Our 2D semiconductors database consisting 130 structures with direct band gap and 358 structures with indirect band gap. We listed the lattice constants, formation energy, Young's modulus, Poisson's ratio at GGA level, as well as the hybrid DFT calculated band gap, ionization energy and electron affinity for each candidate. The remainder of this paper is organized as follows. In Sec. II, methodology and computational details are described. Sec. III presents the calculations of structural, mechanical and electronic properties. Finally, a short summary is given in Sec. IV.

II. METHODOLOGY

A. Density functional calculations

Our total energy and electronic structure calculations were performed using the Vienna Ab initio Simulation Package (VASP).^{34,35} The electron-ion interaction was described using projector augmented wave (PAW) method^{36,37} and the exchange and correlation (XC) were treated with GGA in the Perdew Burke Ernzerhof (PBE) form³⁸. A cutoff energy of 400 eV was adopted for the plane wave basis set, which yields total energies convergence better than 1 meV/atom. In addition, the non-bonding van der Waals (vdW) interaction is incorporated by employing a semi-empirical correction scheme of Grimme's DFT-D2 method in this study unless otherwise stated, which has been successful in describing the geometries of various layered materials.^{39,40}

In the slab model of 2D systems, periodic slabs were separated by a vacuum layer of 20 Å in *c* direction to avoid mirror interactions. In sampling the Brillouin zone integrations, we used Monkhorst-Pack *k*-point meshes with a reciprocal space resolution of $2\pi \times 0.03 \text{ \AA}^{-1}$.⁴¹ On geometry optimization, both the shapes and internal structural parameters of pristine unit-cells were fully relaxed until the residual force on each atom is less than 0.01 eV/Å. Considering that the band gaps of semiconductors are severely underestimated by traditional density functional theory (DFT) calculations with local or semilocal exchange-correlation functionals, part of electronic structure calculations were also performed using the standard Heyd-Scuseria-Ernzerhof (HSE06) hybrid functional, namely the screening parameter $\mu=0.2 \text{ \AA}^{-1}$ and the Hartree-Fock (HF) mixing parameter $\alpha=25\%$ respectively.^{31-33,42-44} Electronic calculations at the HSE06 level were performed upon the PBE-calculated equilibrium geometries.

B. Screening Process

Thermodynamic Stability. First, the formation energies ΔE_f of all investigated 2D systems are investigated to determine their thermodynamic stability. The formation energy of a 2D-system is defined as the energy difference between a material and its pure elemental constituents in their standard state, namely,

$$\Delta E_f = E_{tot} - \sum n_\alpha \mu_\alpha, \quad (1)$$

where E_{tot} is the total energy of pristine 2D system monolayer. n_α is the number of atoms of species α and μ_α is the atomic chemical potential of species α which is equal to the total energy of per atom in its most stable elemental phase. A negative value of ΔE_f for a material means that the thermodynamic stability. In other words, any processes that drive the transformation or decomposition of this material are prohibitive or ki-

netically slow. It is worth noting that the accuracy of the PBE functional for the heat of formation is only around 0.2 eV/atom on average.⁴⁵ Considering that semi-local functionals such as PBE generally underestimate the formation energies of materials, especially for the layered materials. We also note that the PBE-calculated formation energies of Si Ge and Sn monolayer are higher than 0.6 eV/f.u but they have recently been synthesized or isolated by exfoliation.^{22,23,25} Thus, We use a threshold of 1 eV/formula-unit as an upper bound on sufficient thermodynamic stability for the synthesis and growth of free-standing monolayers.

Mechanical Stability. For a 2D crystal, the in-plane stiffness tensor C_{ij} ($i,j=1,2,6$) can be obtained based on the following formula in first-principles calculations,

$$E_s = \frac{1}{2} C_{11} \varepsilon_{xx}^2 + \frac{1}{2} C_{22} \varepsilon_{yy}^2 + C_{12} \varepsilon_{xx} \varepsilon_{yy} + 2C_{66} \varepsilon_{xy}^2, \quad (2)$$

where the tensile strain is defined as $\varepsilon = \frac{a-a_0}{a}$, a and a_0 are the lattice constants of the strained and strain-free structures, respectively. In order to calculate the elastic stiffness constants, the E_s as a function of ε in the strain range $-2\% \leq \varepsilon \leq 2\%$ with an increment of 0.5% are investigated. The elastic constants C_{ij} were obtained by fitting a second-order polynomial to the change on the total energy versus applied strain by post-processing the VASP calculated data using the VASPKIT code.⁴⁶ According to the Born-Huang criteria,⁴⁷ a mechanically stable 2D sheet would satisfy $C_{66} > 0$ and $C_{11}C_{22} - C_{12}^2 > 0$. Then the Young's modulus Y and Poisson's ratio ν can be derived as

$$Y(x) = \frac{C_{11}C_{22} - C_{12}^2}{C_{22}}, \quad Y(y) = \frac{C_{11}C_{22} - C_{12}^2}{C_{11}}, \quad (3)$$

and

$$\nu(x) = \frac{C_{12}}{C_{22}}, \quad \nu(y) = \frac{C_{12}}{C_{11}}, \quad (4)$$

where x and y corresponds to lattice *a* and *b* directions respectively.

Furthermore, the dynamic stability reflects the structural stability when the structure is perturbed, which can be determined by calculating the phonon spectrum of a material using either a finite displacement method⁴⁸ or density functional perturbation theory⁴⁹. If imaginary modes exist in the phonon spectra, implying that this material will undergo reconstructive or martensitic phase transformations after a slight lattice distortion upon it. Finally, the thermal stability reflects the resistance to decomposition at high temperatures (higher room temperature), which can be evaluated by performing ab initio molecular dynamics simulations. Strictly speaking, a stable material must satisfy thermodynamic, mechanical, dynamic and thermal stabilities simultaneously. Considering that the determination of dynamic and thermal stabilities is rather computationally expensive, in our current study we use only thermodynamic and mechanical

stability as two stability criteria to screen the potential 2D materials.

Semiconductor Screening. The band gaps E_g of nonmagnetic semiconductors can be obtained as,

$$E_g = \epsilon_{\text{CBM}} - \epsilon_{\text{VBM}}, \quad (5)$$

where ϵ_{CBM} and ϵ_{VBM} are the Kohn-Sham eigenvalues of conduction-band minimum (CBM) and valence-band maximum (VBM) respectively. It is known that DFT usually underestimates the band gap of semiconductors but yield similar dispersion curves as compared to the HSE06 result. Thus, we first perform the global band structure with a fine resolution of $2\pi \times 0.008 \text{ \AA}^{-1}$ (for example, a 59×59 kmesh for graphene), to locate the positions of valence band maximum (VBM) and conduction band minimum (CBM) for each potential candidate in the reciprocal-space at PBE level. Then we calculate values of both ϵ_{CBM} and ϵ_{VBM} at HSE06 level. In addition to energy gap, ionization energy (IE) and electron affinity (EA) are important parameters for any electronic material. They can be calculated by aligning VBM and CBM with respect to the vacuum level which is determined by aligning the planar-averaged electrostatic potential within the layer with the vacuum region as illustrated in Fig. 1.

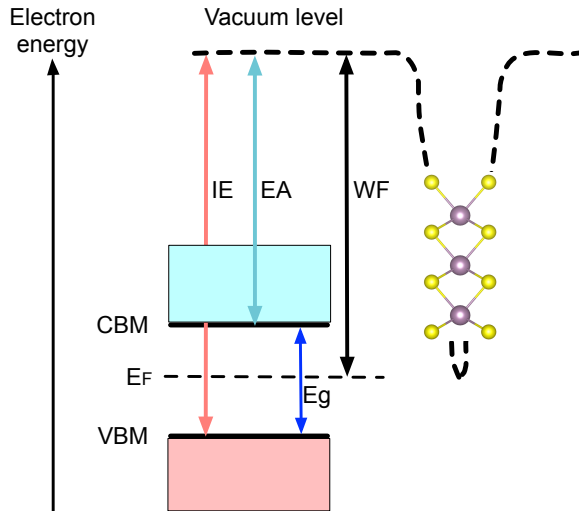


FIG. 1. (Color online) Schematic diagram of ionization energy IE, electron affinity EA and work function WF defined as the VBM, CBM and Fermi level E_F with respect to the vacuum level.

C. High-Throughput Setting

To search for novel 2D semiconductors, we use the VASPKIT package⁵⁰ as a high-throughput interface to pre-process the input files and post-process the calculated

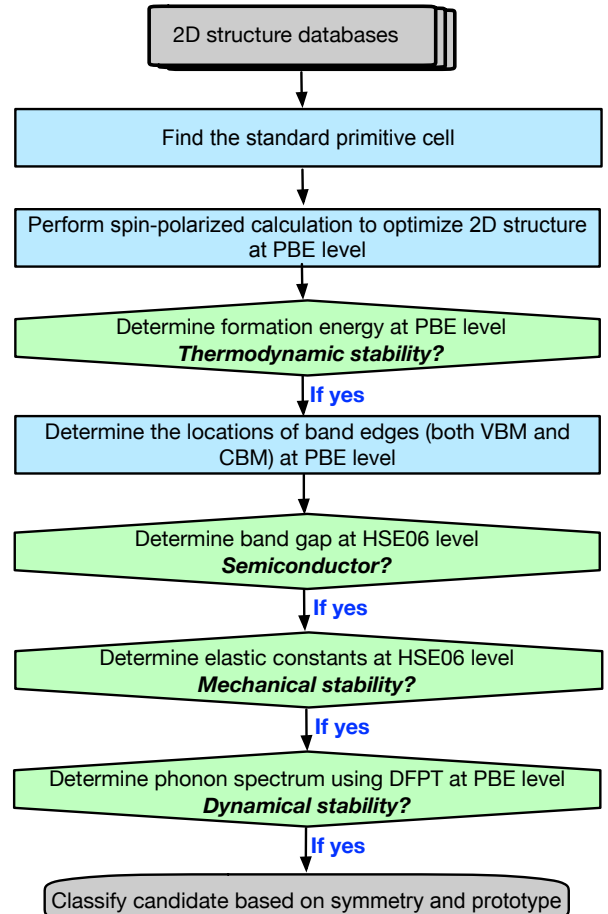


FIG. 2. (Color online) Schematic representation of the fundamental steps needed to find two-dimensional semiconductors.

data obtained by using VASP code. The overview of the screening process is presented in Fig. 2. Firstly, we use the VASPKIT code to generate the other three input files (POTCAR, KPOINTS, and INCAR) when POSCAR is given. Then we perform spin-polarized structural-relaxation calculations at PBE-D2 level to determine the magnetic ground state configuration and formation energy for each 2D material. If the candidate is thermodynamically stable, we next perform the global band structure at PBE level. Considering that the band structure calculation at HSE06 level is a rather time-consuming task, in the determination of band gap E_g , we only perform the static HSE06 calculation at irreducible k-point coordinates but includes the positions of both CBM and VBM in the reciprocal space. At the PBE-calculated lattice constants. Finally, if the candidate is mechanically stable and has a band gap value larger than zero eV, this means that it might be a novel potential 2D semiconductor. We take graphene as an example and present its global band structure in Fig. 3 (a). It is clearly found that the band edges, i.e., both valence band maximum (VBM) and conduction band minimum (CBM) encounter at the K point (1/3, 1/3) to form the Dirac cone. By an-

alyzing the projected band structure and the real-part of wavefunctions of band edges in real space [Figs. 3 (b) and (d)], one can observe that the VBM and CBM to be derived from the bonding π and anti-bonding π^* states respectively, due to the interaction of p_z - p_z orbitals of carbon atoms.

III. RESULTS AND DISCUSSION

We begin our discussion by comparing our predicted data with available experimental reports. Up until now, several monolayers have been successfully exfoliated or synthesized in the experiments, including borophene (Cmmm),⁵¹ graphene (P6/mmm),¹ phosphorene (Pmna),^{12,16,17} silicene (P-3m1),^{19–22} germanene (P-3m1),^{23,24} stanene (P-3m1)²⁵, h-BN (P-6m2)^{18,52}, MoS₂ (P-6m2)¹⁴, TiS₃ (P2₁/m)⁵³. Our results are well agreement with the available experimental and theoretical data. For examples, we reproduce the semi-metallic character of graphene, silicene and germanene, and stanene when ignored the effect of spin-orbit coupling. The PBE-calculated Young's modulus and Poisson's ratio of graphene are 338.69 N·m and 0.17, in excellent agreement with the available values of 340 N·m and 0.186,^{54,55} respectively. The HSE06 calculated band gap of 1.61 eV for phosphorene, 5.70 eV for h-BN, 2.13 eV for MoS₂ and 1.15 eV for TiS₃, well agreement with previous reports.^{14,18,56,57}

Based on the above criteria, 120 direct- and 358 indirect-gap 2D nonmagnetic semiconductors are screened from near 1000 2D monolayers. The PBE-calculated lattice constants, formation energy, Young's modulus, Poisson's ratio, as well as HSE06-calculated band gap, ionization energy and electron affinity for each candidate are listed in the Supplemental Material. Furthermore, The classification of these possible 2D semiconductors is summarized in Fig. 5. One can find that the most of the 2D semiconductors are binary which is predominant by AB₂ structures [Fig. 5(b)]. It should be pointed that transition-metal dichalcogenides

(TMDCs) is one of the most interesting AB₂ layered compounds and display a wide range of important properties. The TMDCs monolayer have three phases, namely, 2H (P-6m2), 1T (P-3m1) and 1T' (P2₁/m) respectively. Previous theoretical studies predicted around 50 different transition-metal oxides (TMOs) and TMDCs can remain stable as either 2H and/or 1T free-standing structures.^{58,59} Although part of these potential MX₂ compounds are absent in their bulk counterparts. For the sake of completeness, we have also revisited the stability and electronic structure of TMOs and TMDCs with three possible phases (2H, 1T and 1T' respectively). There are four typical 2D Bravais lattices, namely, tetragonal, orthorhombic, hexagonal and monoclinic respectively. The Ball-and-stick model, Brillouin zone and band path of band structure for these Bravais lattice in our high-throughput calculation are presented in Fig. 4. It is found that most of the semiconducting candidates belong to orthorhombic and hexagonal Bravais lattices. Furthermore, their band gap magnitude is mainly concentrated between 1.0 eV and 3.0 eV.

IV. SUMMARY

In conclusion, we identified 120 direct- and 358 indirect-gap 2D nonmagnetic semiconductors from near 1000 2D monolayers by performing high-throughput calculations together with density-functional theory. The calculated properties including lattice constants, formation energy, Young's modulus, Poisson's ratio, band gap, band structure, ionization energy and electron affinity are available online for each candidate.

ACKNOWLEDGMENTS

This work is supported by the support of Natural Science Basic Research Plan in Shaanxi Province of China (Program No. 2017JM1008) and by the Institute for Materials Research of Tohoku University for High Performance Computing.

* wangwei@icloud.com.

† geng@ustb.edu.cn.

¹ K. S. Novoselov, A. K. Geim, S. V. Morozov, D. Jiang, Y. Zhang, S. V. Dubonos, I. V. Grigorieva, and A. A. Firsov, *Science* **306**, 666 (2004).

² K. Novoselov, A. K. Geim, S. Morozov, D. Jiang, M. Katsnelson, I. Grigorieva, S. Dubonos, and A. Firsov, *Nature* **438**, 197 (2005).

³ L. Song, Z. Liu, A. L. M. Reddy, N. T. Narayanan, J. Tahatijerina, J. Peng, G. Gao, J. Lou, R. Vajtai, and P. M. Ajayan, *Adv. Mater.* **24**, 4878 (2012).

⁴ Q. H. Wang, K. Kalantar-Zadeh, A. Kis, J. N. Coleman, and M. S. Strano, *Nat. Nano.* **7**, 699 (2012).

⁵ Y. Zhang, Y.-W. Tan, H. L. Stormer, and P. Kim, *Nature* **438**, 201 (2005).

⁶ M. Chhowalla, H. S. Shin, G. Eda, L.-J. Li, K. P. Loh, and H. Zhang, *Nat. Chem.* **5**, 263 (2013).

⁷ M. Xu, T. Liang, M. Shi, and H. Chen, *Chem. Rev.* **113**, 3766 (2013).

⁸ S. Z. Butler, S. M. Hollen, L. Cao, Y. Cui, J. A. Gupta, H. R. Gutierrez, T. F. Heinz, S. S. Hong, J. Huang, A. F. Ismach, E. Johnston-Halperin, M. Kuno, V. V. Plashnitsa, R. D. Robinson, R. S. Ruoff, S. Salahuddin, J. Shan, L. Shi, M. G. Spencer, M. Terrones, W. Windl, and J. E. Goldberger, *ACS Nano* **7**, 2898 (2013).

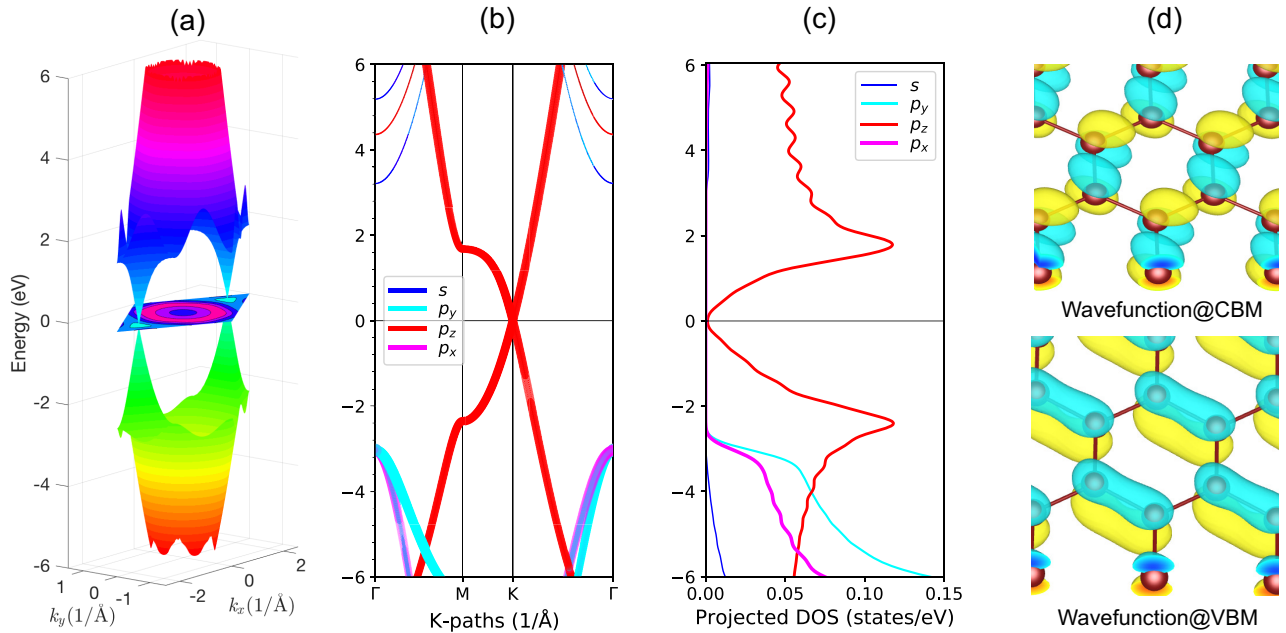


FIG. 3. (Color online) PBE calculated (a) global band structure, (b) projected band structure, (c) projected density of states, and (d) real part of wave function for band edges in graphene.

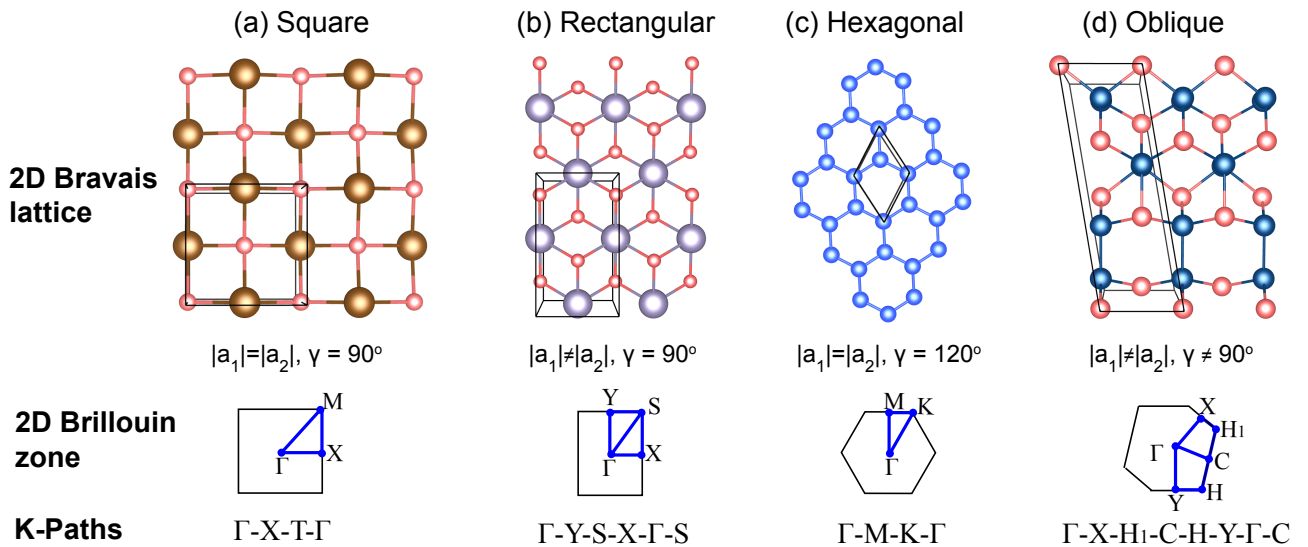


FIG. 4. (Color online) Classification of predicted two-dimensional semiconductors in term of (a) number of chemical constituents, (b) prototypes, (c) lattice type, (d) space group, (e) band gap character and (f) band gap magnitude.

⁹ Q. Zeng, H. Wang, W. Fu, Y. Gong, W. Zhou, P. M. Ajayan, J. Lou, and Z. Liu, *Small* **11**, 1868 (2015).
¹⁰ S. Balendhran, S. Walia, H. Nili, S. Sriram, and M. Bhaskaran, *Small* **11**, 640 (2015).
¹¹ X. Wang, A. M. Jones, K. L. Seyler, V. Tran, Y. Jia, H. Zhao, H. Wang, L. Yang, X. Xu, and F. Xia, *Nat. Nano.* **10**, 517 (2015).
¹² H. Liu, Y. Du, Y. Deng, and P. D. Ye, *Chem. Soc. Rev.* **44**, 2732 (2015).
¹³ H. Wang, H. Yuan, S. Sae Hong, Y. Li, and Y. Cui, *Chem. Soc. Rev.* **44**, 2664 (2015).

¹⁴ K. F. Mak, C. Lee, J. Hone, J. Shan, and T. F. Heinz, *Phys. Rev. Lett.* **105**, 136805 (2010).
¹⁵ S. Manzeli, D. Ovchinnikov, D. Pasquier, O. V. Yazyev, and A. Kis, *Nat. Rev. Mater.* **2**, 17033 (2017).
¹⁶ L. Li, Y. Yu, G. J. Ye, Q. Ge, X. Ou, H. Wu, D. Feng, X. H. Chen, and Y. Zhang, *Nat. Nanotechnol.* **9**, 372 (2014).
¹⁷ H. Liu, A. T. Neal, Z. Zhu, Z. Luo, X. Xu, D. Tománek, and P. D. Ye, *ACS Nano* **8**, 4033 (2014).
¹⁸ K. Watanabe, T. Taniguchi, and H. Kanda, *Nat. Mater.* **3**, 404 (2004).

TABLE I. Calculated lattice constant a , interlayer distance between two adjacent layers Δd , formation enthalpy E_f and band gap E_g for buckled monolayer, bilayer and trilayer of group-III nitrides using PBE, HSE06 and G0W0 approaches respectively.

Bravais Lattice	Label and coordinates of specific points	Bravais Lattice	Label and coordinates of specific points
Square	$\Gamma (0, 0)$ $\mathbf{X} (\frac{1}{2}, 0)$ $\mathbf{M} (\frac{1}{2}, \frac{1}{2})$	Oblique	$\Gamma (0, 0)$ $\mathbf{X} (\frac{1}{2}, 0)$ $\mathbf{Y} (0, \frac{1}{2})$
Hexagonal	$\Gamma (0, 0)$ $\mathbf{K} (\frac{1}{3}, \frac{1}{3})$ $\mathbf{M} (\frac{1}{2}, 0)$	Oblique	$\mathbf{C} (\frac{1}{2}, \frac{1}{2})$ $\mathbf{H} (\eta, 1-\nu)^a$ $\mathbf{H}_1 (1-\eta, \nu)^a$
Rectangular	$\Gamma (0, 0)$ $\mathbf{Y} (0, \frac{1}{2})$	Rectangular	$\mathbf{X} (\frac{1}{2}, 0)$ $\mathbf{S} (\frac{1}{2}, \frac{1}{2})$

^a $\eta = \frac{1-acos\gamma/b}{2sin^2\gamma}$ and $\nu = \frac{1}{2} - \frac{\eta bcos\gamma}{a}$.

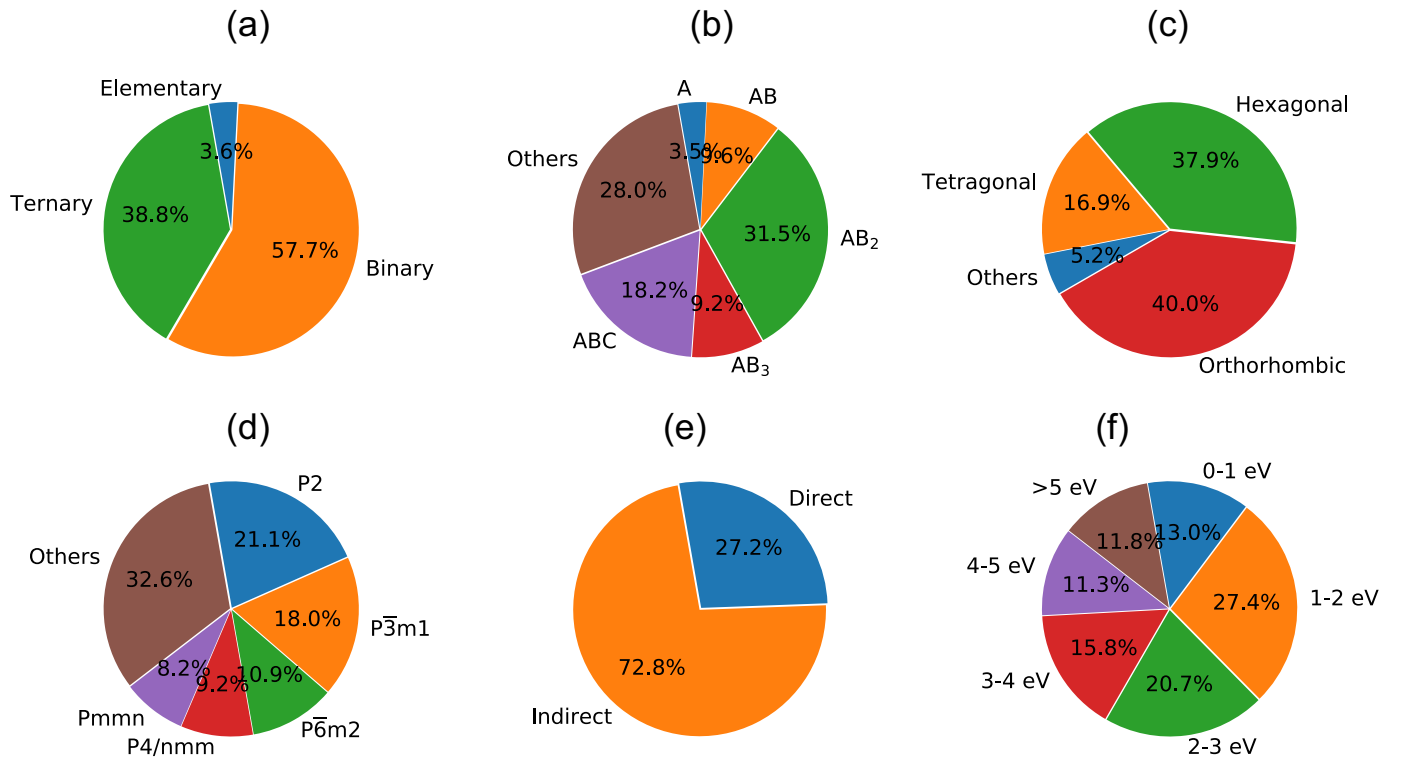


FIG. 5. (Color online) Classification of predicted two-dimensional semiconductors in term of (a) number of chemical constituents, (b) prototypes, (c) lattice type, (d) space group, (e) band gap character and (f) band gap magnitude.

¹⁹ Y. Sugiyama, H. Okamoto, T. Mitsuoka, T. Morikawa, K. Nakanishi, T. Ohta, and H. Nakano, *JACS* **132**, 5946 (2010).
²⁰ H. Okamoto, Y. Kumai, Y. Sugiyama, T. Mitsuoka, K. Nakanishi, T. Ohta, H. Nozaki, S. Yamaguchi, S. Shirai, and H. Nakano, *JACS* **132**, 2710 (2010).
²¹ A. O'Hare, F. Kusmartsev, and K. Kugel, *Nano Lett.* **12**, 1045 (2012).
²² P. Vogt, P. De Padova, C. Quaresima, J. Avila, E. Frantzeskakis, M. C. Asensio, A. Resta, B. Ealet, and G. Le Lay, *Phys. Rev. Lett.* **108**, 155501 (2012).
²³ E. Bianco, S. Butler, S. Jiang, O. D. Restrepo, W. Windl, and J. E. Goldberger, *ACS Nano* **7**, 4414 (2013).
²⁴ L. Li, S.-z. Lu, J. Pan, Z. Qin, Y.-q. Wang, Y. Wang, G.-y. Cao, S. Du, and H.-J. Gao, *Adv. Mater.* **26**, 4820 (2014).
²⁵ F.-f. Zhu, W.-j. Chen, Y. Xu, C.-l. Gao, D.-d. Guan, C.-h. Liu, D. Qian, S.-C. Zhang, and J.-f. Jia, *Nat. Mater.* **14**, 1020 (2015).
²⁶ T. Inoshita, S. Jeong, N. Hamada, and H. Hosono, *Phys. Rev. X* **4**, 031023 (2014).
²⁷ M. Ashton, J. Paul, S. B. Sinnott, and R. G. Hennig, *Phys. Rev. Lett.* **118**, 106101 (2017).

²⁸ A. Jain, S. P. Ong, G. Hautier, W. Chen, W. D. Richards, S. Dacek, S. Cholia, D. Gunter, D. Skinner, G. Ceder, and K. A. Persson, *APL Mater.* **1**, 011002 (2013).

²⁹ K. Choudhary, I. Kalish, R. Beams, and F. Tavazza, *Sci. Rep.* **7**, 5179 (2017).

³⁰ N. Mounet, M. Gibertini, P. Schwaller, D. Campi, A. Merkys, A. Marrazzo, T. Sohier, I. E. Castelli, A. Cepellotti, G. Pizzi, and N. Marzari, *Nat. Nanotechnol.* **13**, 246 (2018).

³¹ J. Heyd, G. E. Scuseria, and M. Ernzerhof, *J. Chem. Phys.* **118**, 8207 (2003).

³² A. V. Krukau, O. A. Vydrov, A. F. Izmaylov, and G. E. Scuseria, *J. Chem. Phys.* **125**, 224106 (2006).

³³ M. Marsman, J. Paier, A. Stroppa, and G. Kresse, *J. Phys.: Condens. Matter* **20**, 064201 (2008).

³⁴ G. Kresse and J. Furthmüller, *Phys. Rev. B* **54**, 11169 (1996).

³⁵ G. Kresse and J. Furthmüller, *Comput. Phys. Sci.* **6**, 15 (1996).

³⁶ P. E. Blöchl, *Phys. Rev. B* **50**, 17953 (1994).

³⁷ G. Kresse and D. Joubert, *Phys. Rev. B* **59**, 1758 (1999).

³⁸ J. P. Perdew, K. Burke, and M. Ernzerhof, *Phys. Rev. Lett.* **77**, 3865 (1996).

³⁹ S. Grimme, *J. Comput. Chem.* **27**, 1787 (2006).

⁴⁰ T. Bučko, J. Hafner, S. Lebègue, and J. Ángyán, *J. Phys. Chem. A* **114**, 11814 (2010).

⁴¹ H. J. Monkhorst and J. D. Pack, *Phys. Rev. B* **13**, 5188 (1976).

⁴² A. D. Becke, *J. Chem. Phys.* **98**, 1372 (1993).

⁴³ J. P. Perdew, M. Ernzerhof, and K. Burke, *J. Chem. Phys.* **105**, 9982 (1996).

⁴⁴ J. Paier, M. Marsman, K. Hummer, G. Kresse, I. C. Gerber, and J. G. Angyan, *J. Chem. Phys.* **124**, 154709 (2006).

⁴⁵ M. Pandey and K. W. Jacobsen, *Phys. Rev. B* **91**, 235201 (2015).

⁴⁶ V. Wang and W.-T. Geng, *J. Phys. Chem. C* **121**, 10224 (2017).

⁴⁷ M. Born and K. Huang, “Dynamic theory of crystal lattice, clarendon,” (1954).

⁴⁸ K. Parlinski, Z. Q. Li, and Y. Kawazoe, *Phys. Rev. Lett.* **78**, 4063 (1997).

⁴⁹ S. Baroni, S. de Gironcoli, A. Dal Corso, and P. Giannozzi, *Rev. Mod. Phys.* **73**, 515 (2001).

⁵⁰ V. Wang, “VASPKIT, a pre- and post-processing program for the VASP code,” (2018).

⁵¹ A. J. Mannix, X.-F. Zhou, B. Kiraly, J. D. Wood, D. Alducin, B. D. Myers, X. Liu, B. L. Fisher, U. Santiago, J. R. Guest, M. J. Yacaman, A. Ponce, A. R. Oganov, M. C. Hersam, and N. P. Guisinger, *Science* **350**, 1513 (2015).

⁵² D. Paciliçœ, J. C. Meyer, İ. G. Girit, and A. Zettl, *Appl. Phys. Lett.* **92**, 133107 (2008).

⁵³ J. O. Island, M. Barawi, R. Biele, A. Almazığen, J. M. Clamagirand, J. R. Ares, C. Sütçüenchez, H. S. J. van der Zant, J. V. İ.çelvarez, R. D’Agosta, I. J. Ferrer, and A. Castellanos?Gomez, *Adv. Mater.* **27**, 2595 (2015).

⁵⁴ C. Lee, X. Wei, J. W. Kysar, and J. Hone, *Science* **321**, 385 (2008).

⁵⁵ F. Liu, P. Ming, and J. Li, *Phys. Rev. B* **76**, 064120 (2007).

⁵⁶ V. Wang, Y. Kawazoe, and W. T. Geng, *Phys. Rev. B* **91**, 045433 (2015).

⁵⁷ D. Jun, L. Ming, and Z. X. Cheng, *WIREs Comput. Mol. Sci.* **6**, 211 (2016).

⁵⁸ C. Ataca, H. ?ahin, and S. Ciraci, *J. Phys. Chem. C* **116**, 8983 (2012).

⁵⁹ F. A. Rasmussen and K. S. Thygesen, *J. Phys. Chem. C* **119**, 13169 (2015).

⁶⁰ K. S. Novoselov, D. Jiang, F. Schedin, T. J. Booth, V. V. Khotkevich, S. V. Morozov, and A. K. Geim, *PNAS* **102**, 10451 (2005).

⁶¹ B. Radisavljevic, A. Radenovic, J. Brivio, V. Giacometti, and A. Kis, *Nat. Nanotechnol.* **6**, 147 (2011).

⁶² F. Schwierz, *Nature Nanotech.* **5**, 487 (2010).

⁶³ A. Balushi, Y. Zakaria, K. Wang, R. K. Ghosh, R. A. Vila, S. M. Eichfeld, J. D. Caldwell, X. Qin, Y.-C. Lin, P. A. DeSario, G. Stone, S. Subramanian, D. F. Paul, R. M. Wallace, S. Datta, J. M. Redwing, and J. A. Robinson, *Nat. Mater.* **15**, 1166 (2016).

⁶⁴ W. R. L. Lambrecht and B. Segall, *Phys. Rev. B* **47**, 9289 (1993).

⁶⁵ F. H?o?eser, T. Olsen, and K. S. Thygesen, *Phys. Rev. B* **88**, 245309 (2013).

⁶⁶ S. Kirklin, J. E. Saal, B. Meredig, A. Thompson, J. W. Doak, M. Aykol, S. R?o?ehl, and C. Wolverton, *NPJ Comput. Mater.* **1**, 15010 (2015).

⁶⁷ S. Curtarolo, W. Setyawan, S. Wang, J. Xue, K. Yang, R. H. Taylor, L. J. Nelson, G. L. Hart, S. Sanvito, M. Buongiorno-Nardelli, N. Mingo, and O. Levy, *Comput. Mater. Sci.* **58**, 227 (2012).

⁶⁸ J. O. Island, M. Barawi, R. Biele, A. Almazığen, J. M. Clamagirand, J. R. Ares, C. Sütçüenchez, H. S. J. van der Zant, J. V. İ.çelvarez, R. D’Agosta, I. J. Ferrer, and A. Castellanos?Gomez, *Adv. Mater.* **27**, 2595 (2015).